

PACS numbers: 42.81.Cn; 42.25.Fx
DOI: 10.1070/QE2011v041n10ABEH014695

Angular distribution of light scattered from heavily doped silica fibres

V.V. Alekseev, M.E. Likhachev, M.M. Bubnov, M.Yu. Salganskii,
V.F. Khopin, A.N. Gur'yanov, E.M. Dianov

Abstract. **This paper describes an experimental setup for precision measurements of the angular distribution of light scattered by optical fibres in a wide angular range and demonstrates that the models of anomalous scattering proposed to date need to be refined. We have found and interpreted a discrepancy between the Rayleigh scattering coefficients measured by different techniques.**

Keywords: *fibre optics, heavily doped fibres, light scattering, anomalous scattering, Rayleigh scattering coefficient.*

1. Introduction

Single-mode silica optical fibres doped with high concentrations of various oxides are used in a variety of nonlinear devices: Raman lasers and amplifiers [1], parametric amplifiers [2] and nonlinear switches [3]. The efficiency of such devices can be raised substantially by increasing the nonlinearity of the fibre via an increase in the doping level of the fibre core. This is, however, accompanied by a considerably more rapid increase in optical loss, which makes it impossible to reach the highest possible efficiency of the device. As shown earlier, losses in heavily doped fibres are contributed by light scattering at the core–cladding interface [4] and in the region of the central dip in the refractive-index profile [5]. This type of scattering is referred to as anomalous. To describe it, Rawson [6, 7] proposed and developed a model of light scattering by microfluctuations of the core–cladding interface.

The origin of such microfluctuations is not yet understood. This paper examines two possible mechanisms. One mechanism stems from the fact that, when a preform is drawn into fibre, the core–cladding boundary in the hot zone (in the region of the drawing cone) is the interface between two liquids differing in viscosity. The hydrodynamic instability of the interface gives rise to microdeviations from its mean position [8, 9]. Disturbances of the core–cladding interface were observed during preform collapse and were named viscosity fingers [10]. The other possible mechanism assumes that the interface is disturbed by capillary waves that emerge during fibre drawing and are of thermodynamic origin [11]. We attempted to separately evaluate the contributions of these competing mechanisms by analysing the shape of the angular distribution of anomalous scattering, which carries information about the size distribution of inhomogeneities and their cross-sectional position in the fibre. To this end, we have developed a technique that ensures high sensitivity and high resolution in scattered-light distribution measurements over the entire angular range (0–180°).

V.V. Alekseev, M.E. Likhachev, M.M. Bubnov, E.M. Dianov Fiber Optics Research Center, Russian Academy of Sciences, ul. Vavilova 38, 119333 Moscow, Russia; e-mail: Alekseev@fo.gpi.ru;
M.Yu. Salganskii, V.F. Khopin, A.N. Gur'yanov Institute of Chemistry of High-Purity Substances, Russian Academy of Sciences, ul. Tropinina 49, 603950 Nizhnii Novgorod, Russia

Received 20 July 2011; revision received 12 September 2011
Kvantovaya Elektronika **41** (10) 917–923 (2011)
Translated by O.M. Tsarev

2. Experimental

2.1. Setup for scattered-light angular distribution measurements

A schematic of the experimental setup for scattered-light distribution measurements is shown in Fig. 1. A key part of the setup is a KU silica cell (*1*) in the shape of a semi-cylinder (bounded by a cylindrical surface and a plane passing through the axis of the cylinder). A stripped fibre (*3*) placed in a cuvette (*2*) is parallel to the flat surface (Π) of the cell. The light scattered in direction φ and coupled out from the fibre into the cylinder at the same angle is apertured by a slit (*4*) of width D. The cylinder surface acts as a lens, with a photodetector (*5*) at its focal point. The propagation of rays in the cylinder is such that the focal point locus is a circle of radius R, concentric with the surface of the cylinder. The photodetector is translated along this circle, whose radius is given by

$$R = nr^*/(n-1), \tag{1}$$

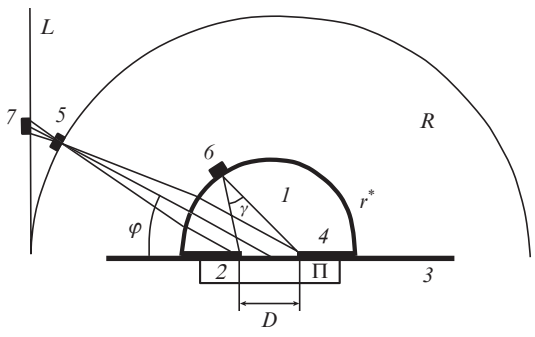

Figure 1. Schematic of the experimental setup for measurements of angular distribution of light scattered from optical fibres: (*1*) silica semicylinder; (*2*) cuvette filled with an immersion liquid; (*3*) fibre; (*4*) aperture of width D; (*5*, *6*, *7*) photodetectors (position in this study and in Refs [6, 5], respectively).

where r^* is the radius of the cylinder and n is the refractive index of silica. In our setup, r^* was 3 cm. The resolution of the system is determined by the spherical aberration of the cylindrical lens and depends on the aperture size, D. The system has the lowest resolution when the scattering angle is $\varphi = 90°$. At other angles, the resolution is better because the angular size of the aperture as viewed from the position of the photodetector has a maximum at $\varphi = 90°$. Curves (*1*) and (*2*) in Fig. 2 show the angular resolution of the system as a function of relative aperture size, $D/2r^*$. As seen, at $D/2r^* = 0.3$ the lowest resolution of the system is ~1° at a scattering angle $\varphi = 90°$. At other scattering angles, the resolution is better.

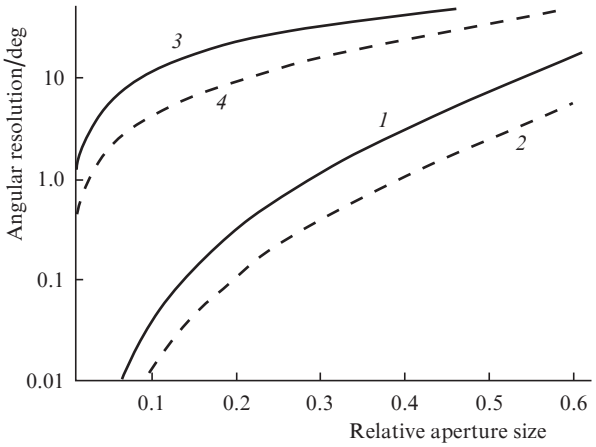

Figure 2. Angular resolution as a function of relative aperture size, $D/2r^*$, at scattering angles of (*1*, *3*) 90° and (*2*, *4*) 20°; (*1*, *2*) this work, (*3*, *4*) [6].

Comparison with previous scattered-light distribution measurements highlights the advantages of the proposed measurement geometry. In Ref. [6], a photodetector (*6*) was translated along the surface of the cylinder (Fig. 1). In this geometry, there is no beam focusing effect, the photodetector receives the light scattered throughout an angular range of width γ (Fig. 1), and it is this angle that determines the resolution of the system. Just as in our setup, it depends on D and scattering angle [Fig. 2, curves (*3*, *4*)]. It can be seen that, to reach a resolution of ~1° (as in our setup), the size of the visible area in Ref. [6] should have been reduced by 30 times, which would lead to an equivalent reduction in signal-to-noise ratio. In the setup reported by Likhachev et al. [5], a photodetector (*7*) was translated along a straight line (L) tangent to the circle R (Fig. 1). Increasing the distance from the tangency point, situated at the focus, led to signal defocusing and, accordingly, the resolution degraded rapidly. At $D/2r^* = 0.3$ and $\varphi = 10°$, 25° and 40°, the resolution was about 1°, 2° and 5°, respectively. The maximum scattering angle in that geometry depended on the aperture size [5] and was in practice limited to 30°–60° because, with increasing φ, the centre of the beam spot (*7*) moved to infinity and the spot broadened.

The light source used in our setup was a Nd:YAG laser ($\lambda = 1.064$ μm) with a linearly polarised output. The light coupled into the fibre was modulated at 1 kHz and ranged in power from 100 to 200 mW. The scattered light was monitored by a synchronous detector. Since the scattered light intensity may depend on polarisation direction, measurements were made at several azimuthal directions of the fibre, and the results were averaged. In addition, the measurement results were averaged over the length of the fibre. Note that all of the fibres studied were sufficiently homogeneous, and the measured angular distribution of scattered light varied little from region to region.

The proposed technique allows calibration of the measured angular distribution of scattered light in order to evaluate the absolute scattering loss. To this end, we measured light scattering in multimode germanosilicate fibres, in which Rayleigh scattering greatly prevails over anomalous scattering in almost the entire angular range. Figure 3 shows a measured and a calculated angular distribution of light scattered from a Ge651mm multimode germanosilicate fibre with a core diameter of 62.5 μm. The dips in scattered light intensity near 0 and 180° are due to the scattered-light capture in the fibre core through the total internal reflection at the core–cladding interface, which was taken into account in our angular distribution calculations.

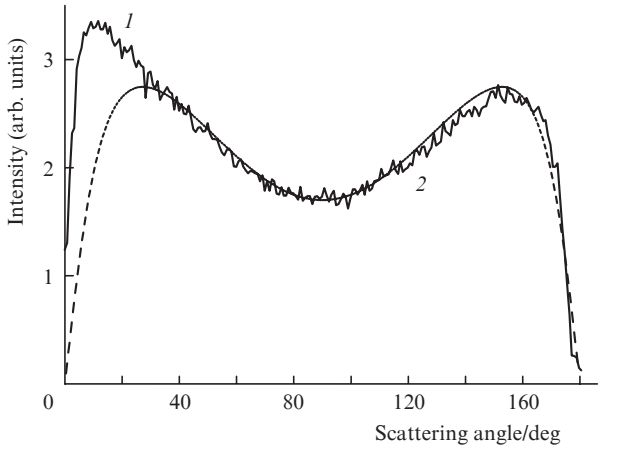

Figure 3. Angular distributions of scattered light for sensitivity calibration of the experimental setup: (*1*) distribution for a Ge651mm multimode germanosilicate fibre, (*2*) calculated distribution at $\Delta n = 0.018$.

The absolute Rayleigh scattering intensity in the multimode fibres used for calibration can be determined through independent Rayleigh scattering coefficient measurements using λ^{-4} analysis of the optical loss spectrum of the fibre [12] or from known Rayleigh scattering coefficients of the core material [13]. The method used allows sensitivity calibration of the experimental setup and determination of the total scattering loss in the fibre with an accuracy of 5%–7%.

2.2. Optical fibres

As shown earlier [4, 5], anomalous scattering is contributed primarily by the core–cladding interface and the region of the central dip in the refractive-index profile. To study the scattering in the region of the core–cladding interface, we used two fibre preforms with the central dip eliminated in the fabrication stage. The germania-doped core of the preforms had a step-index profile. The core–cladding index difference, Δn, was 0.035 in the Ge303 preform and 0.040 in the Ge304 preform. The preforms were drawn into fibres under different conditions. It follows from earlier results [4] that anomalous scattering in these fibres occurs in the region of the core–clad-

ding interface. In all the fibres, the small-angle anomalous scattering level (see e.g. Fig. 4a) was two orders of magnitude above the Rayleigh scattering level, and the total optical loss due to anomalous scattering was an order of magnitude above the Rayleigh scattering loss.

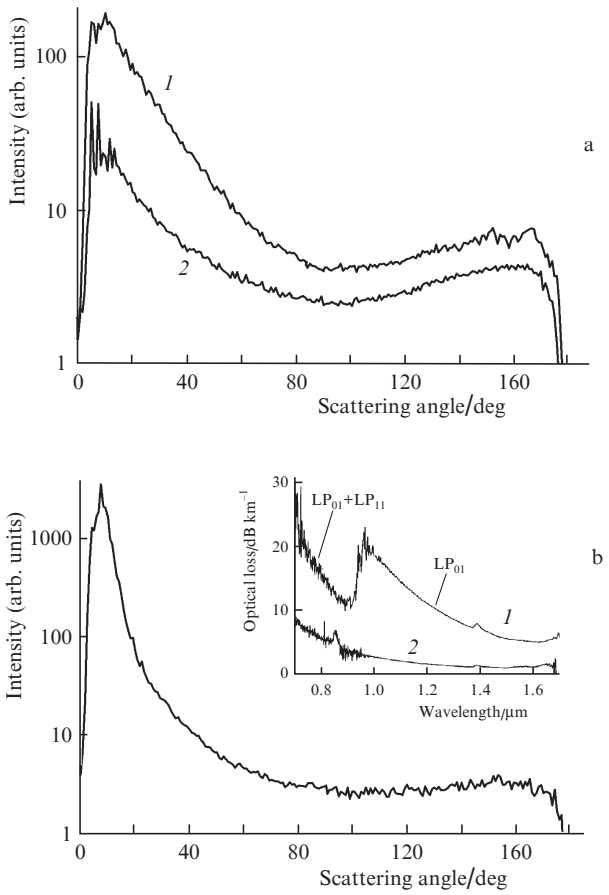

Figure 4. Angular distributions of light scattered from fibres (a) (*1*) Ge303sm, (*2*) Ge303mm and (b) P926. Inset: optical loss spectra of (*1*) P926 and (*2*) an analogous fibre with no central dip.

To study the scattering in the region of the central dip in the index profile, we fabricated several fibres with increased scattering in this region. It is worth noting that this type of scattering is relatively weak in conventional heavily doped fibres. In particular, completely eliminating the central dip reduces the optical loss in fibres containing 30 mol% GeO_2 by 30% [14]. For this reason, one fails to separately assess the angular distribution of light scattering due to the central dip in such fibres, because the scattering in the region of the core–cladding interface is twice as strong. In connection with this, we changed collapse conditions in the preform fabrication stage, which led to changes in the region of the central dip in the index profile. In this way, we fabricated the preform for the phosphosilicate fibre P926, whose refractive-index profile is shown in the inset in Fig. 6b.

Analysis of the optical loss spectrum of P926 indicated a significant (twofold) increase in optical loss in going from few-mode to single-mode operation [Fig. 4b, inset, spectrum (*1*)]. Also shown for comparison in the inset is the optical loss spectrum of an analogous phosphosilicate fibre with no central dip [spectrum (*2*)]. The optical loss in the LP_{01} fundamental mode is seen to considerably exceed that in the LP_{11} mode. Since the fraction of power propagating in the region of the core–cladding interface is greater for the LP_{11} mode, it is obvious that the excess loss originates in the region of the central dip in the index profile, where the intensity of the latter mode is nearly zero. From the loss increase in going to single-mode operation, the characteristic size of the central-dip region responsible for the excess loss can be estimated at ~10% of the core diameter. Angular distribution measurements (Fig. 4b) showed that 65% of the total optical loss in P926 was due to anomalous scattering (10% was accounted for by Rayleigh scattering, and 25%, by absorption). Thus, we have, for the first time, separately assessed the angular distribution of light scattering in the region of the central dip. We assume that the observed strong scattering is due to the formation of an air microcapillary in the central region during the preform collapse process, but we failed to detect it by optical or electron microscopy.

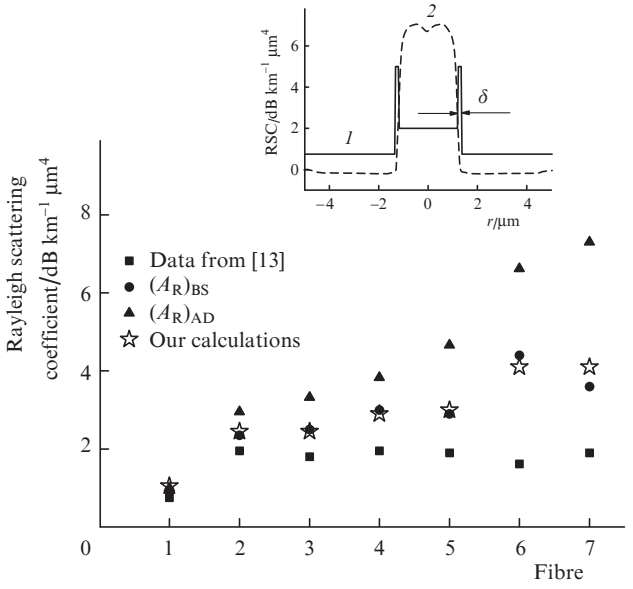

Figure 5. Rayleigh scattering coefficients determined by different techniques. Inset: radial (*1*) RSC and (*2*) index profiles in a fibre.

3. Rayleigh scattering coefficient measurement

The ratio of the outer diameter to core diameter in MCVD preforms is about 8. Fibre drawn out from such a preform will be multimode. To obtain a single-mode heavily doped fibre, the above ratio should be about 50. For this purpose, the starting preform underwent three steps of stretching and overjacketing with a silica tube.

Figure 4a shows the angular distributions of light scattered from a Ge303sm single-mode fibre [curve (*1*)], with increased scattering at the core–cladding interface, and from a Ge303mm multimode fibre [curve (*2*)], drawn from the starting preform. As seen, the angular distributions each can be divided into two portions: one due to anomalous scattering, which prevails in the angular range 0–60°, and the other due to Rayleigh scattering, which prevails in a backscattering geometry (90°–180°). In addition, the Rayleigh scattering level in the single-mode fibre is seen to considerably exceed that in the multimode fibre even though the fraction of power

propagating through the germania-doped core is smaller in the single-mode fibre. The Rayleigh scattering coefficient (RSC) evaluated from the angular distribution of the multimode fibre is equal to the RSC of germanosilicate glass at the given doping level [13]. The RSC extracted from the angular distribution of the single-mode fibre is 100% greater than that reported by Shibata et al. [13].

To gain greater insight into the observed effect, we determined the RSC of seven single-mode fibres using backscattering measurements [15] (Fig. 5). Fibre 1 had a phosphosilicate core ($\Delta n \approx 0.012$) and a low anomalous scattering level. The other fibres had a heavily doped ($\Delta n \approx 0.035-0.040$) germanosilicate core and a step-index profile. Fibre 4 had a central dip in the index profile. The scatter in the RSCs determined by backscattering measurements was mainly due to differences in fibre fabrication conditions. Also shown in Fig. 5 are the RSCs evaluated from the angular distribution of light scattering and from data reported for doped silica glass [13]. In all the fibres that were found to have an increased Rayleigh scattering level in angular distribution measurements, the RSC determined from backscattering measurements also exceeded the RSC in glass of the same composition. The discrepancy between the RSCs determined by the two techniques ranged up to a factor of 2 in some cases.

To accurately describe Rayleigh scattering, one should use the function $A_R(r)$, which represents the radial RSC profile. According to Likhachev et al. [12], the RSC determined from backscattering (BS) measurements is averaged over the fourth power of the field in the fibre:

$$(A_R)_{BS} = \frac{\int_0^\infty A_R(r)\psi_n^4(r)r\mathrm{d}r}{\int_0^\infty \psi_n^4(r)r\mathrm{d}r}, \tag{2}$$

where ψ_n is the near-field distribution (normalised to unity) in the fibre. When the RSC is evaluated from the angular distribution (AD) of light scattering, the average is taken over the square of the field:

$$(A_R)_{AD} = \frac{\int_0^\infty A_R(r)\psi_n^2(r)r\mathrm{d}r}{\int_0^\infty \psi_n^2(r)r\mathrm{d}r} \quad . \tag{3}$$

The fibres studied had increased anomalous scattering at the core–cladding interface. In our opinion, it is this region which is responsible for the increased Rayleigh scattering. The inset in Fig. 5 shows the assumed RSC profile for this case [curve (*1*)] and the index profile across the fibre core [curve (*2*)]. The best agreement between the RSCs calculated by Eqns (2) and (3) was achieved under the assumption that an annular region of increased Rayleigh scattering lies at the core–cladding interface. Taking its width, δ, to be considerably smaller than the core radius and using the RSC of germanosilicate glass [13], we find for the Ge303sm fibre (fibre 3 in Fig. 5) from Eqns (2) and (3)

$$(A_R)_{BS} = 1.73 + 0.15B, \tag{4}$$

$$(A_R)_{AD} = 1.50 + 0.36B, \tag{5}$$

where B is the product of the average RSC in the region of the core–cladding interface, $\langle A \rangle$, with δ (Fig. 5). Eliminating B from the two equations, we obtain a relation between the RSCs determined by the two techniques:

$$(A_R)_{BS} = 1.10 + 0.42(A_R)_{AD}. \tag{6}$$

The Rayleigh scattering coefficient determined from the angular distribution of light scattered by Ge303sm is $(A_R)_{AD} = 3.2$ dB km^{-1} μm^4. Substituting this value into (6), we obtain $(A_R)_{BS} = 2.45$ dB km^{-1} μm^4, in good agreement with the experimentally determined value (2.5 dB km^{-1} μm^4). The calculation results for the approximation used are represented by asterisks in Fig. 5 and completely account for the observed effect. Note that the numerical values of the coefficients in (6) will vary slightly from fibre to fibre.

Increased Rayleigh scattering at the core–cladding interface has been detected for the first time. We assume this scattering to have the following nature: In the preform fabrication process, the average particle size in the deposit is ~120 nm [16]. It is reasonable to expect that the core–cladding boundary, an interface between glasses of different compositions, will be rough rather than smooth, with a characteristic roughness length scale of the same order as the particle size in the deposit. Therefore, because of the large refractive-index difference across the core–cladding interface, strong Rayleigh scattering would be expected at the interface. It is of interest to note that, taken alone, neither of the above RSC determination techniques ensures accurate description of Rayleigh scattering in heavily doped step-index fibres. The Rayleigh scattering intensity in the fibre core and its contribution at the core–cladding interface can only be assessed by combining the two techniques.

4. Angular distribution of anomalous scattering

Figure 6 shows angular distributions of anomalous scattering obtained by subtracting the Rayleigh scattering contribution from the total scattering angular distribution for scattering at the core–cladding interface and in the region of the central dip in the refractive-index profile. It is worth noting that, because the angular distributions for the fibres with increased scattering at the core–cladding interface differed little in shape, we examined in detail only the angular distribution for Ge303sm. In contrast to earlier studies of anomalous scattering [5, 6, 17], we were able to assess light scattering in a wide angular range, where the scattering intensity varied over almost two orders of magnitude. There is obvious interest in interpreting the measured angular distributions in terms of anomalous scattering models proposed to date.

The best agreement between the calculation and measurement results was achieved with a model that considers light scattering by randomly distributed spatial fluctuations of the core–cladding interface [18]. In this model, the scattered light intensity is given by

$$I(\varphi) = \frac{k^4\sigma^2a^2\Delta^4}{2\pi^3}\left(\frac{ncE_a^2}{8\pi}\right)(1+\cos^2\varphi)\,T(\varphi)$$

$$\times\int_0^{L_0}(L_0-u)R_{cor}(u)\cos[ku(\cos\varphi-1)]\mathrm{d}u\times$$

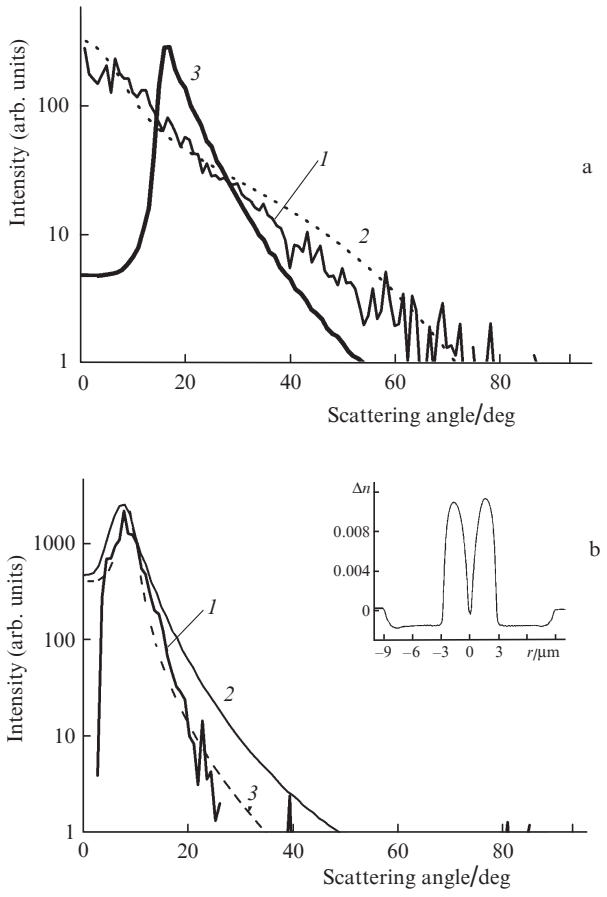

Figure 6. Angular distributions of anomalous scattering (a) at the core–cladding interface and (b) in the region of the central dip;
(a) (*1*) experiment; (*2*) calculation using Eqns (7)–(9) with L_{cor} = 0.5 μm, V_{cor} = 0.6 rad and a = 1.3 μm; (*3*) calculation in the temperature wave model; (b) (*1*) experiment; (*2*) calculation in the temperature wave model; (c) calculation in the hydrodynamic instability model with α = 0.025 μm^{-1} and β = 0.1 μm^{-1} in Eqn (10). Inset: refractive-index profile of P926.

$$\times\int_0^{\pi\sqrt{2}} dw \int_0^{w} S_{cor}(\theta)\cos\left(2ka\sin\varphi\sin\frac{w}{\sqrt{2}}\sin\frac{\theta}{\sqrt{2}}\right)d\theta, \quad (7)$$

where k is the wavenumber in the core; σ is the rms fluctuation amplitude; a is the core radius; $\Delta = \Delta n/n$ is the relative refractive index of the fibre core; E_a is the electric field at the core–cladding interface; L_0 is the fibre length over which the scattered light is collected; $T(\varphi)$ takes into account the fraction of light captured in the core; and $R_{cor}(u)$ and $S_{cor}(\theta)$ are normalised autocorrelation functions for axial and azimuthal interface deviations.

Mazunder et al. [18] used Gaussian autocorrelation functions,

$$R_{cor}(u) = \exp(-u^2/L_{cor}^2), \quad (8)$$

$$S_{cor}(\theta) = \exp(-\theta^2/V_{cor}^2), \quad (9)$$

which corresponds to a simple stochastic process with no periodic component.

Curve (*2*) in Fig. 6a represents the angular distribution of scattered light calculated by Eqns (7)–(9) with L_{cor} and V_{cor} adjusted to give the best fit for the experimental data. As seen, the width and slope of the angular distribution are represented only approximately, and the best fit curve differs in shape from the measured distribution, especially when the scattering intensity decreases by 10 to 100 times (at large scattering angles). The angular distribution of light scattering in the region of the central dip in the index profile (Fig. 6b) cannot be represented using formulas derived by Mazunder et al. [18]. The measured angular distribution has a maximum at a scattering angle near 10° and differs from calculated curves at any values of L_{cor} and V_{cor} (the calculation procedure is described below).

That the measured angular distributions are poorly fitted by Eqns (7)–(9) is most likely due to the fact that the correlation functions (8) and (9) are chosen for the simplest stochastic process and, hence, are unrelated to the actual physical mechanism behind the development of inhomogeneities at the core–cladding interface and in the region of the central dip.

To calculate the shape of the angular distribution for the capillary wave mechanism, we used results reported by Roberts et al. [11]. According to the capillary wave model considered by them, the amplitude of capillary waves depends on their spatial frequency, ω. As shown in Ref. [11], the spectral density of the roughness amplitude, ζ, is inversely proportional to the spatial frequency, ω, of the roughness component. The maximum value of ζ is determined by the cutoff frequency, ω_0.

Knowing $\zeta(\omega)$ and applying the inverse Fourier transformation, one can find a characteristic form of deviation as a function of longitudinal coordinate along the core–cladding interface and construct autocorrelation functions. Substituting the functions into (7), we can calculate the shape of the angular distribution of scattered light as a function of cutoff frequency, ω_0, as was done in this study.

Curve (*3*) in Fig. 6a represents the angular distribution that was calculated in this way and is the most similar in shape to the measured angular distribution of light scattering at the core–cladding interface. The discrepancy between the calculated and measured distributions is seen to be even greater than that in the case of stochastic variations proposed by Mazunder et al. [18]. The approach in question gives somewhat better results for scattering in the region of the central dip (Fig. 6b), but the calculated distribution [curve (*2*)] is broader than the measured one [curve (*1*)].

Clearly, when the hydrodynamic instability model is used, scattering at the core–cladding interface and that in the region of the central dip should be considered separately. Indeed, in the former case we deal with flow of the viscous glass of the silica tube, which contains doped glass with lower viscosity. This problem is on the whole similar to that of instability of a stretching viscous liquid jet [9], with the only difference that here instability develops on the outer jet surface, whereas we are interested in cross-sectional interface variations on the inner surface of a stretching viscous cylindrical jet. This problem is in general rather difficult to solve, especially because of viscosity variations (due to the variation in glass temperature across the heating zone), and is beyond the framework of this paper. A direct comparison of calculated and measured angular distributions of light scattering at the core–cladding interface is thus problematic.

In the latter case, we deal with the problem of variations in the position and shape of a rather viscous central dip in a less viscous liquid (core glass). In the limit of very high glass viscosity in the region of the central dip and very low viscosity

of the core glass, the problem can be treated as that of variations in the position of a thread (central dip) in a viscous liquid. It is reasonable to expect that such variations will have the form of damped harmonic oscillations:

$$\eta \sim e^{-\alpha z}\cos(\beta z), \quad (10)$$

where z is a coordinate along the fibre axis, and α and β are constants. Formula (10) can be used to calculate the correlation function and angular distribution of light scattering. Adjusting α and β as fitting parameters, we were able to represent the small-angle portion of the angular distribution of anomalous scattering in P926 [Fig. 6b, curve (*3*)]. Thus, the assumption that the position of the central dip varies as a result of hydrodynamic instability proves true.

5. Discussion

Measurements on model fibres allowed us to identify two types of anomalous scattering, differing in angular distribution: scattering at the core–cladding interface and that in the region of the central dip in the refractive-index profile. The assumption that there is anomalous scattering by capillary waves on the interface between liquids differing in viscosity is inconsistent with the present experimental data: it gives no way of describing the shape of the observed angular distributions. However, the observed discrepancy between the measured and calculated distributions cannot be considered conclusive evidence against scattering by capillary waves. Indeed, Roberts et al. [11] derived the spectral density of the roughness amplitude as a function of spatial frequency for a glass–air interface, rather than for an interface between two glasses of different compositions. Moreover, the low-frequency cutoff, ω_0, needs to be accurately determined.

At the same time, our results demonstrate that scattering in the region of the central dip can be described in terms of a hydrodynamic model as oscillations of a thread (the central dip, formed by a lightly doped, high-viscosity glass) in a less viscous liquid (molten core glass). A more complex situation occurs with scattering in the region of the core–cladding interface. On the one hand, it is well known that the flow of an elongating viscous jet, uniform or containing an interface between liquids differing in viscosity, is unstable [9, 19]. On the other, the corresponding equations are rather complex and, because of the variable flow viscosity (due to the variation in temperature across the heating zone), cannot be used in the framework of this paper to calculate the shape of the angular distribution or to compare it to the experimentally determined shape.

On the whole, it appears unlikely that the anomalous scattering in the region of the central dip and that at the core–cladding interface are due to fundamentally different mechanisms. The above considerations lead us to conclude that the most likely origin of scattering centres is the hydrodynamic instability of interfaces between glasses of different compositions in the fibre drawing process. It is worth recalling the observed Rayleigh scattering from the core–cladding interface. It is due to the interface roughness, which most likely arises during the preform fabrication process because the particles being deposited have a finite size. It may be that it is such nonuniformities that act as seeds for the development of interfacial nonuniformities during the drawing process, which give rise to anomalous scattering. This assumption is supported by the following fact: fluorine doping of the core using freon reduces the optical loss due to anomalous scattering in heavily doped step-index germanosilicate fibres, whereas doping to the same fluorine concentration using SiF_4 does not [16]. According to our results, in the former case freon reacts with the particles being deposited, reducing their size and, accordingly, the size of fluctuations of the core–cladding interface, whereas in the latter case the particle size remains unchanged [16].

6. Conclusions

A new technique has been developed for measuring the angular distribution of scattered light using optical fibres with increased scattering in the regions of the core–cladding interface and central dip. This enabled the first precision measurement of the angular distribution of scattered light in these regions.

Rayleigh scattering has been found for the first time at the core–cladding interface in step-index fibres, and the discrepancy between the RSCs determined in different ways (from the angular distribution of scattering and using backscattering measurements) has been accounted for.

Analysis of the possible origins of scattering nonuniformities around the core–cladding interface and in the region of the central dip in the index profile indicates that the model that considers the development of capillary waves on the interface between liquids of different compositions gives no way of describing the shape of the observed angular distributions, whereas assuming hydrodynamic instability of a viscous liquid flow we were able to describe the angular distribution of scattered light in the region of the central dip.

Acknowledgements. This work was supported in part by the Russian Foundation for Basic Research (Grant No. 10-02-01334-a).

References

1. Sudo S., Itoh H. *Opt. Quantum Electron.*, **22**, 187 (1990).
2. Solodyankin M.A., Guryanov A.N., Kazantseva N.A., Khopin V.F., Bubnov M.M., Likhachev M.E., Dianov E.M. *Laser Phys. Lett.*, **2**, 190 (2005).
3. Kravtsov K.S., Prucnal P.R., Bubnov M.M. *Opt. Express*, **15**, 13114 (2007).
4. Likhachev M.E., Bubnov M.M., Semenov S.L., Khopin V.F., Salganskii M.Yu., Gur'yanov A.N., Dianov E.M. *Kvantovaya Elektron.*, **34**, 241 (2004) [*Quantum Electron.*, **34**, 241 (2004)].
5. Likhachev M.E., Bubnov M.M., Semenov S.L., Khopin V.F., Salganskii M.Yu., Gur'yanov A.N., Dianov E.M. *Kvantovaya Elektron.*, **36**, 464 (2006) [*Quantum Electron.*, **36**, 464 (2006)].
6. Rawson E. *Appl. Opt.*, **11**, 2477 (1972).
7. Rawson E. *Appl. Opt.*, **13**, 2370 (1974).
8. Frankel I., Weihs D. *J. Fluid Mech.*, **185**, 361 (1987).
9. Chesnokov Yu.G. *Prikl. Mekh. Tekh. Fiz.*, **42**, 56 (2001).
10. Biriukov A.S., Dianov E.M., Kurkov A.S., Khitun A.G., Devyatykh G.G., Gur'yanov A.N., Gusovskii D.D., Kobis S.V. *Proc. SPIE–Int. Soc. Opt. Eng.*, **3211**, 309 (1998).
11. Roberts P.J., Couny F., Sabert H., Mangan B.J., Williams D.P., Farr L., Mason M.W., Tomlinson A., Birks T.A., Knight J.C., Russell P.St.J. *Opt. Express*, **13**, 236 (2005).
12. Likhachev M.E., Semenov S.L., Khopin V.F., Salganskii M.Yu., Zen'kovskii G.V., Bubnov M.M. *Issled. Ross.*, **8**, 67 (2005). http://zhurnal.ape.relarn.ru/articles/2005/008.pdf
13. Shibata N., Kawachi M., Edahiro T. *Trans. Inst. Electron. Commun. Eng. Jpn.*, **E63**, 837 (1980).
14. Bubnov M.M., Semjonov S.L., Likhachev M.E., Dianov E.M., et al. *IEEE Photonics Technol. Lett.,* **16** (8), 1870 (2004).

15. Hartog A.H., Gold M.P. *J. Lightwave Technol.*, **LT-2**, 76 (1984).
16. Bubnov M.M., Guryanov A.N., Dianov E.M., Ketkova L.A., Likhachev M.E., Salganskii M.Yu., Khopin V.F. *Neorg. Mater.*, **46**, 626, (2010).
17. Lines M.E., Reed W.A., DiGiovanni D.J., Hamblin J.R. *Electron. Lett*., **35**, 1009 (1999).
18. Mazunder P., Logunov S., Raghavan S. *J. Appl. Phys*., **96**, 4042 (2004).
19. Grant M., Desai C.R. *Phys. Rev. A*, **27**, 2577 (1983).